PHYSICAL REVIEW B 68, 094111 (2003)

# Electron paramagnetic resonance and electron-nuclear double resonance study of trapped-hole centers in $LiB_3O_5$ crystals

Wei Hong, M. M. Chirila, N. Y. Garces, and L. E. Halliburton*
*Physics Department, West Virginia University, Morgantown, West Virginia 26506, USA*

D. Lupinski and P. Villeval
*Cristal Laser S.A., 12 Allee Jean Rostand, 54230 Chaligny, France*

(Received 29 December 2002; revised manuscript received 7 April 2003; published 17 September 2003)

Electron paramagnetic resonance (EPR) and electron-nuclear double resonance (ENDOR) have been used to characterize two distinct hole centers in single crystals of $LiB_3O_5$ (commonly referred to as LBO). Irradiating a crystal at 77 K with x rays produces an intense four-line holelike EPR signal, with the structure arising from the hyperfine interaction with one $^{11}B$ nucleus. Warming the crystal to approximately 130 K destroys the first hole center and allows a second less intense four-line holelike EPR signal to be observed (also interacting with one $^{11}B$ nucleus). The second hole center decays between 150 and 200 K. EPR and ENDOR angular dependence data were used to determine the $g$ matrix and the $^{11}B$ hyperfine and nuclear quadrupole matrices for each hole center. We suggest that the first (less thermally stable) center is a self-trapped hole. In this defect, the hole is localized primarily on an oxygen ion between a threefold bonded boron and a fourfold bonded boron, and the self-trapping occurs because of a significant relaxation of the neighboring fourfold boron away from the hole. GAUSSIAN 98 calculations, using a $(B_3O_7H_4)^0$ cluster to represent the defect and the nearby lattice, support this self-trapping mechanism. A similar model is suggested for the second hole center, except in this case a neighboring lithium vacancy is included to provide the increased thermal stability. These trapped-hole centers are of interest because of their possible role in the unwanted transient optical absorption produced in $LiB_3O_5$ crystals at room temperature by high-power pulsed ultraviolet lasers.

DOI: 10.1103/PhysRevB.68.094111 PACS number(s): 61.72.Ji, 76.30.Mi, 76.70.Dx, 42.70.Mp

## I. INTRODUCTION

Lithium triborate ($LiB_3O_5$), better known as LBO, is a widely used nonlinear optical material. It has a wide ultraviolet transmission range, a relatively high optical damage threshold, and a moderate nonlinear optical coefficient.[1,2] These unique properties, when combined with excellent mechanical hardness and chemical stability, make lithium triborate the material of choice for a variety of harmonic generation and optical parametric oscillator applications in the ultraviolet, visible, and near infrared. As is often the case with laser materials, point defects in the $LiB_3O_5$ crystals can affect the performance of devices, especially when highly energetic photons are present. High-power laser systems, incorporating $LiB_3O_5$ as a nonlinear optical element and operating in a pulsed mode with one or more beams in the ultraviolet, can produce unwanted transient absorption bands in the $LiB_3O_5$ crystals that extend from below 200 nm to above 400 nm.[3] These transient absorption bands are believed to occur when "free" holes and electrons formed by two-photon or three-photon absorption events (a result of high laser power) become temporarily localized in the lattice, either self-trapped or trapped at pre-existing defect sites such as lithium and oxygen vacancies. Minimizing the transient absorption phenomenon, and thus optimizing the overall device performance of this nonlinear optical material, requires a complete understanding of all the point defects in lithium triborate.

In an early investigation of $LiB_3O_5$, Scripsick *et al.*[4] used electron paramagnetic resonance (EPR), electron-nuclear double resonance (ENDOR), optical absorption, and thermoluminescence to determine the effects of ionizing radiation. They found that two prominent paramagnetic centers, one holelike and the other electronlike, appeared when a device-quality crystal was irradiated with x rays at 77 K. A broad optical absorption band peaking near 300 nm was formed at the same time. Subsequent heating caused the induced EPR signals and the absorption to decay in the 100–150 K range, with an accompanying thermoluminescence glow peak near 126 K. This early report on point defects in single crystals of $LiB_3O_5$ has been accompanied and followed by a series of in-depth studies[3,5–12] initiated by Ogorodnikov and coworkers at Ural State Technical University and involving collaborators at other institutions. Many of their efforts have focused on the luminescence properties of $LiB_3O_5$, and they have used both electron beams and synchrotron radiation as excitation sources to study the time-resolved nature of the emissions. In addition to these various defect-related studies, there have also been several reports of first-principle calculations of the electronic structure and nonlinear optical properties of regular unperturbed $LiB_3O_5$ crystals.[13–20]

In the present paper, we describe the results of an EPR and ENDOR study of two trapped hole centers in single crystals of $LiB_3O_5$. The first of these hole centers (which we label Hole Center *A*) is produced at 77 K by an x-ray irradiation. This center thermally decays near 130 K and a second hole center (labeled Hole Center *B*) is then observed. Each center has a large interaction with one boron neighbor, and ENDOR is used to determine complete sets of $^{11}B$ hyperfine and nuclear quadrupole parameters. Both centers con-

 

sist of a hole localized primarily at one oxygen ion. Self-trapping occurs in Hole Center *A* because of a strong lattice relaxation of one of the two boron ions neighboring the hole. The major hyperfine interaction with only one boron, instead of nearly equal interactions with two borons, requires this significant lattice relaxation. A similar defect model is proposed for Hole Center *B*, but with the addition of a nearby lithium vacancy to provide greater thermal stability.

In their preliminary study of what is now referred to as Hole Center *A*, Scripsick *et al.*[4] took EPR and ENDOR data only along one high-symmetry crystal direction and, thus, did not determine the principal values and the principal axes of the *g* matrix and the $^{11}B$ hyperfine and nuclear quadrupole matrices. Based on their limited set of data, these investigators tentatively suggested that the center had the hole localized on an oxygen ion adjacent to a stabilizing entity such as a lithium vacancy. With much more data, we now recognize that the model suggested by Scripsick *et al.*[4] corresponds to Hole Center *B*. Porotnikov *et al.*[6] and Ogorodnikov *et al.*[12] have also reported EPR results from a hole center in $LiB_3O_5$. They did not perform ENDOR experiments and they did not provide $^{11}B$ hyperfine and nuclear quadrupole parameters. Furthermore, their principal values for the *g* matrix deviate significantly from the results in the present paper. In all of these earlier studies of hole centers in $LiB_3O_5$,[4,6,12] the important question of why there is only one large boron hyperfine, instead of similar large interactions with two boron ions, was not addressed.

## II. EXPERIMENTAL DETAILS

The crystal structure[21,22] of $LiB_3O_5$ is orthorhombic (space group $Pna2_1$) with $a=8.447$ Å, $b=7.3789$ Å, and $c=5.1408$ Å. We are using the convention followed by the nonlinear optical community, but an equivalent description can be based on the $Pn2_1a$ space group where the *b* and *c* axes are interchanged relative to our choice. This crystal has 36 atoms in a unit cell; these separate into four sets of nine atoms that transform into each other according to the symmetry elements of the crystal. In general, the $LiB_3O_5$ lattice has one lithium site, three inequivalent boron sites, and five inequivalent oxygen sites. The $LiB_3O_5$ crystals used in our investigation were grown in France (at Cristal Laser) and in China (at Fujian Castech Crystals). Samples for the EPR and ENDOR experiments were rectangular in shape and had nominal dimensions of $2.5\times3\times3.5$ mm$^3$ along the *a*, *b*, and *c* axes, respectively. The trapped hole centers were produced in our samples by irradiating for 30 min at 77 K with x rays (60 kV, 30 mA).

The EPR data were obtained using a Bruker ESP 300 spectrometer operating near 9.45 GHz with a $TE_{102}$ rectangular cavity and 100-kHz static field modulation. A Varian E-500 digital gaussmeter was used to measure the magnetic field and a Hewlett-Packard 5340A counter was used to measure the microwave frequency. A small MgO:Cr crystal was used to correct for the difference in magnetic field between the $LiB_3O_5$ sample and the gaussmeter probe (the isotropic *g* value for $Cr^{3+}$ in MgO is 1.9800). The Bruker ESP 300 spectrometer also was used to obtain the ENDOR data. In these experiments, a $TE_{011}$ cylindrical cavity was used and the rf field was frequency modulated at 12.5 kHz. An Oxford Instruments ESR-900 helium-gas flow system maintained the sample temperature in the 8–60 K region while taking EPR and ENDOR data, and also was used to anneal samples between 80 and 200 K without removing them from the cavity. The ENDOR coil was helical and was attached to the Oxford Instruments glassware extending through the ENDOR cavity.

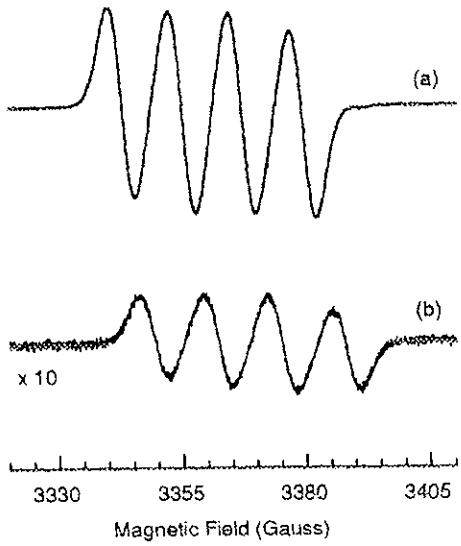


FIG. 1. The *b*-axis EPR spectra of trapped hole centers in $LiB_3O_5$. Hole Center *A* (trace *a*) was taken at 45 K after a 77-K irradiation with x rays. The crystal was held at 130 K for 5 min, and then Hole Center *B* (trace *b*) was taken at 8 K. The lower spectrum has been enhanced by a factor of 10 to allow easier comparison.

## III. RESULTS

Irradiating a $LiB_3O_5$ crystal at 77 K with x rays produces one large holelike EPR spectrum and one electronlike EPR spectrum, both with $S=1/2$. The holelike spectrum is shown in Fig. 1(a). These data were taken at 45 K, with the magnetic field along the *b* axis of the crystal and a microwave frequency of 9.45 GHz. The preliminary ENDOR study by Scripsick *et al.*[4] demonstrated that the resolved four-line hyperfine pattern in this spectrum is due to an interaction with a $^{11}B$ nucleus ($I=3/2$, 80.2% abundant). In the remainder of the present paper, we will refer to the defect responsible for the EPR spectrum in Fig. 1(a) as Hole Center *A*. The radiation-induced electronlike EPR spectrum is shown in Fig. 2. Compared to Fig. 1(a), the data in Fig. 2 were taken with a larger modulation amplitude, a lower microwave power, and a slightly higher temperature. A large (approximately 120 G) hyperfine interaction with one $^{11}B$ nucleus is the major feature in this electronlike spectrum, and the responsible defect is believed to be an oxygen vacancy with an unpaired electron localized primarily on one of the two neighboring boron ions.[4]

After being formed at 77 K with x rays, Hole Center *A* becomes thermally unstable when the $LiB_3O_5$ crystal is held near 130 K for 5 min. A second $S=1/2$ hole center, also with a four-line hyperfine pattern caused by a $^{11}B$ nucleus, is

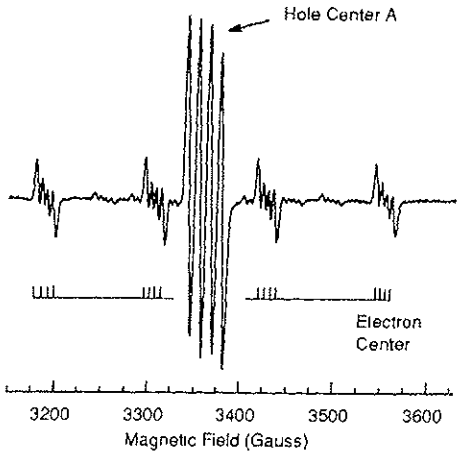


FIG. 2. EPR spectrum showing Hole Center *A* (in the central portion of the scan) and the electronlike center (with the larger 120-G splitting). The data were taken at 60 K with the magnetic field parallel to the b axis.

observed when Hole Center *A* disappears. This second center thermally decays when the temperature reaches the 150–200 K region. The EPR spectrum from this second hole center, taken at 8 K with the magnetic field along the *b* axis, is shown in Fig. 1(b). We will, from now on, refer to the defect responsible for the EPR spectrum in Fig. 1(b) as Hole Center *B*. Because Hole Center *B* is a smaller signal than Hole Center *A*, we have enhanced the spectrum representing Hole Center *B* in Fig. 1(b) by a factor of 10 to allow easier comparison. The similarities in the EPR spectra from Hole Center *A* and Hole Center *B* strongly suggest that the two defects are only slightly modified versions of the same basic structure. The only significant difference between the two centers concerns the optimum temperature to best observe their EPR signals (near 45 K for Hole Center *A* and near 8 K for Hole Center *B*) and arises because Hole Center *A* has a considerably longer spin-lattice relaxation time.

One possible scenario to explain the formation of Hole Center *B* follows. When the anneal temperature approaches 130 K, holes that were initially trapped in the form of Hole Center *A* begin to migrate through the lattice. A majority of these holes encounter an electron trapped next to an oxygen vacancy, where they recombine and restore the crystal to its preirradiated state. However, a small portion of these migrating holes (about 5% in our crystals) encounter a stabilizing entity, where they become trapped and form Hole Center *B*. In an alternative scenario, it is possible that Hole Center *B* is formed during the initial 77-K irradiation, but its EPR spectrum is not easily detected immediately after that irradiation because of the presence of the much larger overlapping signal from Hole Center *A*. In this latter case, Hole Center *B* is observed only after the thermal anneal to near 130 K has removed Hole Center *A*.

A complete set of angular dependence data (both EPR and ENDOR) was collected for Hole Center *A*. Figure 3 shows the EPR results used to determine the *g* matrix. The discrete data points in this figure represent the magnetic field values measured at the middle of each set of hyperfine lines in the EPR spectra, and the solid lines are computer-generated us-

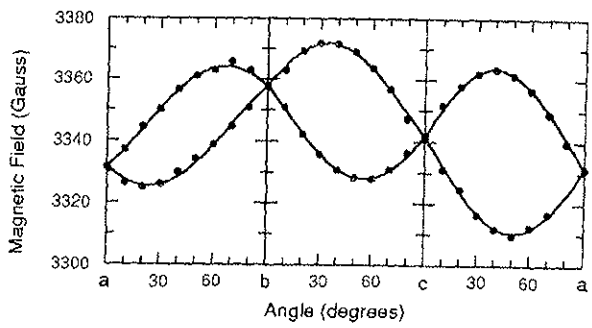


FIG. 3. EPR data showing the angular dependence arising from the *g* matrix for Hole Center *A*. Results are presented for all three high-symmetry planes. Hyperfine splittings are not included.

ing the "best" values obtained for the *g*-matrix parameters. In general, for an arbitrary direction of the magnetic field, there are four magnetically inequivalent, but crystallographically equivalent, orientations (i.e., sites) for Hole Center *A*. These four become pairwise degenerate when the magnetic field is restricted to the *a*-*b*, *b*-*c*, and *c*-*a* planes, as shown in Fig. 3. All four sites are degenerate when the magnetic field is along the *a*, *b*, or *c* axes.

The experimental data in Fig. 3 were fit to a spin Hamiltonian containing only an electron Zeeman term. Values of the *g* matrix parameters for Hole Center *A* are given in Table I. Because there are two sets of parameters that equally well fit the in-plane data shown in Fig. 3, an EPR measurement was made at one out-of-plane orientation of the magnetic field to determine which was the correct set. The directions of the principal axes are specified by $(\theta, \phi)$ pairs of angles, where the polar angle $\theta$ is measured relative to the $+c$ direction and the azimuthal angle $\phi$ is measured relative to the $+a$ direction in the *c* plane with positive rotation being from $+a$ to $+b$. Note that the principal-axis directions given in Table I correspond to only one of the four possible sites for Hole Center *A*. The principal values are the same for each of the four sites, but the principal-axis directions vary for each site since they must reflect the symmetry elements of the $LiB_3O_5$ lattice. The pairs of angles needed to describe the directions of the principal axes at the other three sites are obtained from the initial site as follows.

Site 1: $(\theta, \phi)$
Site 2: $(\theta, 180° - \phi)$ Reflection in the *a* plane
Site 3: $(\theta, 360° - \phi)$ Reflection in the *b* plane
Site 4: $(\theta, 180° + \phi)$ Reflections in both planes

Typical ENDOR spectra representing the primary $^{11}B$ interaction for Hole Center *A* are shown in Fig. 4. These data were taken at 40 K with the magnetic field along the *b* axis of the crystal. The spectrum in Fig. 4(a) was taken while sitting on the higher field line of the two middle lines in the EPR spectrum, and the spectrum in Fig. 4(b) was taken while sitting on the lower field line of the two middle EPR lines. As demonstrated by Scripsick *et al.*,[4] the ENDOR spectra from this center show significant splittings due to a nuclear quadrupole interaction, and the specific ENDOR lines observed in a particular scan depend on which EPR line is selected. Thus, the combined spectra in Fig. 4 illustrate the two sets of three lines each that are expected for an interac-

TABLE I. Experimentally determined principal values and principal axis directions of the $g$ matrices, the hyperfine matrices, and the nuclear quadrupole matrices for Hole Center $A$ and Hole Center $B$ in $LiB_3O_5$. These principal-axis directions correspond to one of the four possible symmetry-related sites of each center. Error limits for the $g$, $A$, and $Q$ parameters are $\pm 0.0003$, $\pm 0.01$ MHz, and $\pm 0.005$ MHz, respectively. Error limits for the $\theta$ and $\phi$ angles associated with $g$ and $A$ are $\pm 0.5°$. Error limits for the $\theta$ and $\phi$ angles associated with $Q$ are $\pm 2°$.

| | | Principal values | Principal-axis directions $\theta$ | $\phi$ |
|---|---|---|---|---|
| **Hole Center** $A$ | | | | |
| | $g_1$ | 2.0021 | 50.5° | 259.1° |
| $g$ | $g_2$ | 2.0101 | 62.4° | 143.6° |
| | $g_3$ | 2.0456 | 51.9° | 29.4° |
| | $A_1$ | −34.49 MHz | 56.8° | 266.2° |
| $A(^{11}B)$ | $A_2$ | −38.53 MHz | 53.4° | 147.2° |
| | $A_3$ | −19.84 MHz | 54.0° | 24.6° |
| | $Q_1$ | −0.138 MHz | 40° | 350° |
| $Q(^{11}B)$ | $Q_2$ | −0.288 MHz | 82° | 250° |
| | $Q_3$ | 0.426 MHz | 51° | 153° |
| **Hole Center** $B$ | | | | |
| | $g_1$ | 2.0016 | 59.8° | 259.9° |
| $g$ | $g_2$ | 2.0102 | 52.6° | 143.5° |
| | $g_3$ | 2.0569 | 52.0° | 16.9° |
| | $A_1$ | −36.62 MHz | 61.4° | 263.1° |
| $A(^{11}B)$ | $A_2$ | −41.39 MHz | 53.8° | 149.6° |
| | $A_3$ | −21.16 MHz | 49.5° | 20.9° |
| | $Q_1$ | −0.167 MHz | 40° | 320° |
| $Q(^{11}B)$ | $Q_2$ | −0.258 MHz | 97° | 239° |
| | $Q_3$ | 0.425 MHz | 51° | 155° |

tion with one $^{11}B$ nucleus. These two quadrupole-split triplet sets of ENDOR lines are, to a first approximation, centered at $A/2$ and separated by $2\nu_N$ (where $\nu_N$, the "free" nuclear resonance frequency, is equal to $g_N\beta_N B/h$). The experimentally observed separation of 9.173 MHz in Fig. 4 is in good agreement with the expected $2\nu_N$ value of 9.231 MHz for the $^{11}B$ nucleus (at a magnetic field near 3378 G). Hole Center $A$ has additional ENDOR lines at lower rf frequencies, as shown in Fig. 5. These data were taken at 30 K with the magnetic field parallel to the $a$ axis of the crystal, and they represent weaker interactions with neighboring lithium and boron nuclei. The largest of these interactions, illustrated by the stick diagram in Fig. 5, is due to one nearby $^7Li$ nucleus. This set of ENDOR lines consists of two barely resolved triplets located near 2.60 and 8.43 MHz (i.e., they are centered at $\nu_N$ and separated by $A$). Their center position of 5.51 MHz agrees well with the 5.48 MHz value of $\nu_N$ expected for a $^7Li$ nucleus (for a magnetic field of 3316 G). The slight splitting of approximately 0.05 MHz within each of the triplets is due to a small nuclear quadrupole interaction.

The angular dependence of the ENDOR spectra representing the primary $^{11}B$ hyperfine interaction associated with Hole Center $A$ is shown in Fig. 6. The discrete points are

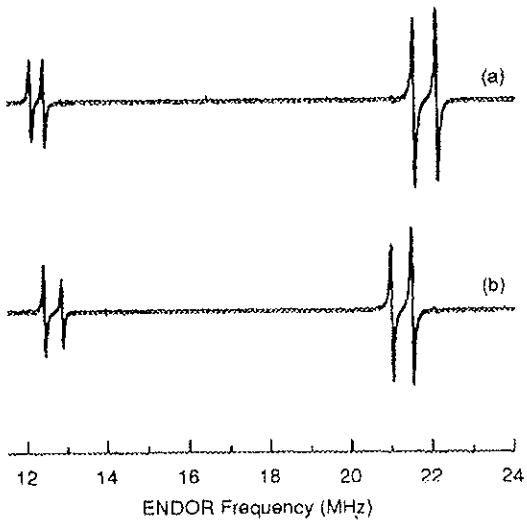


FIG. 4. ENDOR spectra from Hole Center $A$ illustrating the primary $^{11}B$ interactions. Data were taken at 40 K with the magnetic field along the $b$ axis of the crystal. (a) The magnetic field was set on the next to highest EPR line (of the set of four EPR lines). (b) The magnetic field was set on the next to lowest EPR line.

measured frequencies, and the solid lines are computer-generated using the "best" set of values obtained for the hyperfine parameters. These ENDOR data in Fig. 6 contain information about the anisotropy of both the $g$ matrix and the $^{11}B$ hyperfine matrices (i.e., since a different magnetic field was used for each of the angles where ENDOR data were taken). We have fit the data in Fig. 6 using the following spin Hamiltonian and the appropriate $g_N$ value for the $^{11}B$ nucleus:

$$\mathbf{H} = \beta \mathbf{S}\cdot\mathbf{g}\cdot\mathbf{B} + \mathbf{I}\cdot\mathbf{A}\cdot\mathbf{S} + \mathbf{I}\cdot\mathbf{Q}\cdot\mathbf{I} - g_N\beta_N\mathbf{I}\cdot\mathbf{B}. \qquad (1)$$

These terms in the spin Hamiltonian have their usual definitions.[23] The fitting procedure that was used to deter-

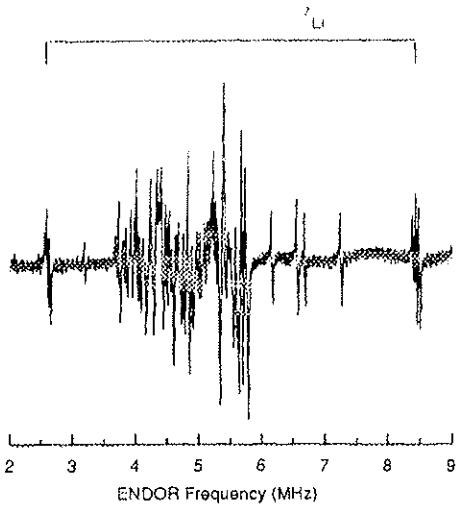


FIG. 5. Low-frequency ENDOR spectrum from Hole Center $A$ showing weak interactions with neighboring lithium and boron nuclei. Data were taken at 30 K with the magnetic field along the $a$ axis. The stick diagram represents the set of ENDOR lines from the nearest-neighbor $^7Li$ nucleus.

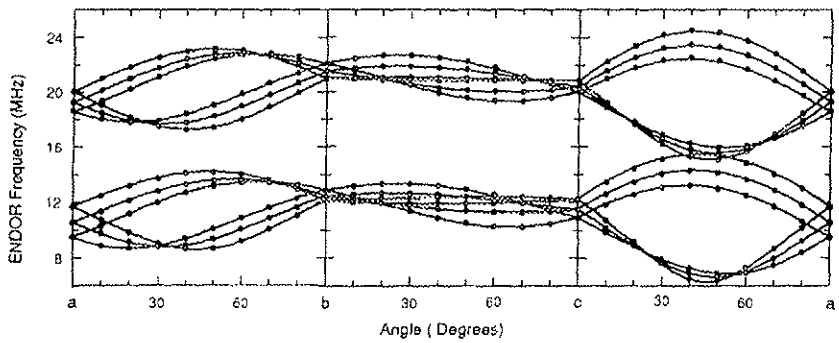


FIG. 6. ENDOR data showing the angular dependence of the primary $^{11}B$ interactions for Hole Center $A$. Results are presented for each of the three high-symmetry planes.

mine the $A$ and $Q$ matrices involved repeated diagonalizations of the $8\times8$ Hamiltonian matrix ($S=1/2$, $I=3/2$). During these "fitting" runs, the parameters describing the $g$ matrix were fixed at the values given in Table I. An ENDOR spectrum was taken at one out-of-plane orientation of the magnetic field to determine the correct final set of $^{11}B$ hyperfine parameters, from a choice of two sets that fit the in-plane data shown in Fig. 6. The "best" values of the primary $^{11}B$ hyperfine and nuclear quadrupole parameters for Hole Center $A$ are listed in Table I. As was done earlier for the $g$ matrix, the directions of the principal axes for the $A$ and $Q$ matrices are specified in Table I by $(\theta,\phi)$ pairs of angles.

The absolute signs of the hyperfine and nuclear quadrupole principal values for Hole Center $A$ (see Table I) cannot be determined directly from the EPR and ENDOR angular data. We do know, however, from the experimental data in Fig. 6 that the signs of $A_1$, $A_2$, and $A_3$ are the same (i.e., these three parameters are all positive or they are all negative). Also, the data in Fig. 4 tells us that $Q_1$ and $Q_2$ have the same signs as $A_1$, $A_2$, and $A_3$. There are several observations that lead us to suggest that the signs given in Table I are the correct set of absolute signs for the principal values of Hole Center $A$. First, we note that the isotropic part of the hyperfine matrix has an "anomalous" sign (i.e., the sign is opposite to that of $g_N$) for many of the trapped hole centers in oxide materials,[24–26] including boron-associated[27] and aluminum-associated centers.[28] This phenomenon has been attributed to a core-polarization mechanism.[29] If a similar behavior occurs for Hole Center $A$ in $LiB_3O_5$, then its hyperfine principal values should all have negative signs (since $g_N$ is positive for the $^{11}B$ nucleus). Note that the same argument will also apply to Hole Center $B$. Second, strong support for negative signs for the principal values of the hyperfine matrix comes from our GAUSSIAN 98 cluster calculations described in the following section. In these calculations, a negative Fermi contact parameter is predicted for the primary $^{11}B$ interaction associated with Hole Center $A$.

The EPR and ENDOR spectra from Hole Center $B$ (observed in a $LiB_3O_5$ crystal after an initial irradiation with x rays at 77 K and a subsequent anneal near 130 K) also have been studied as a function of angle. Figure 7 shows the angular dependence of the $g$ matrix, and Fig. 8 shows the angular dependence of the primary $^{11}B$ hyperfine and nuclear quadrupole interactions. These data were acquired in all three high-symmetry planes. A comparison of Figs. 3 and 7 (for the $g$ matrices) and a comparison of Figs. 6 and 8 (for the $^{11}B$ interactions) show that Hole Center $A$ and Hole Center $B$ are similar. Spin-Hamiltonian parameters for Hole Center $B$ were extracted from these data in Figs. 7 and 8, following the same procedure as for Hole Center $A$. The "best" values for the parameters are included in Table I. Because of the smaller concentration of Hole Center $B$, we did not obtain usable ENDOR data from weak interactions with other neighboring nuclei.

## IV. DISCUSSION

We have acquired the EPR and ENDOR spectra from two very similar hole centers in single crystals of $LiB_3O_5$. Hole Center $A$ is formed during an irradiation at 77 K with x rays, and becomes thermally unstable when the crystal is heated to approximately 130 K. Hole Center $B$, the more stable of the two, is observed after the first center has been thermally destroyed. Combining the experimentally determined spin-Hamiltonian parameters and geometry-optimized quantum-mechanical cluster calculations allows us to establish models for these two hole centers. In this section, we begin with the structure of the perfect lattice and the basic anionic group, then describe the physical constraints introduced by the EPR and ENDOR results, and finally present the results from our cluster calculations.

The 36 atoms that form a unit cell of $LiB_3O_5$ can be divided into four related sets of nine atoms each. Starting with one set of nine atom positions, it is possible to generate another set of nine atom positions by applying one of the transformations representing a symmetry element of the crystal (these three elements are two glide planes and a screw axis). The lattice positions given in Table II correspond to

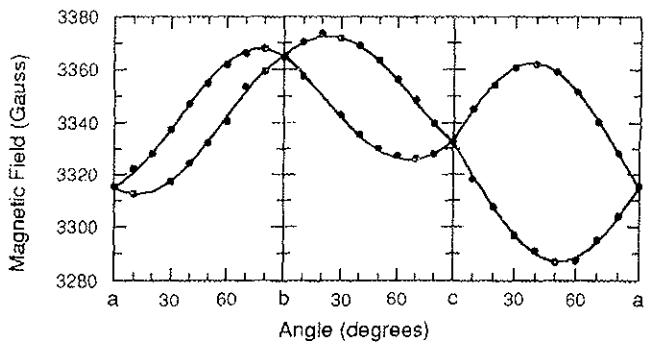


FIG. 7. EPR data showing the angular dependence arising from the $g$ matrix for Hole Center $B$. Results are presented for all three high-symmetry planes. Hyperfine splittings are not included.

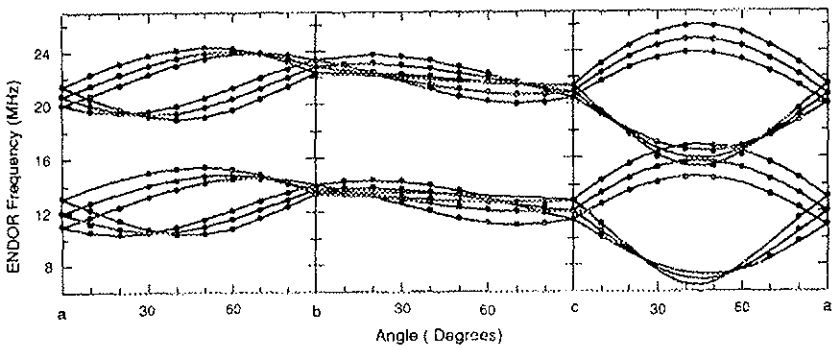


FIG. 8. ENDOR data showing the angular dependence of the primary $^{11}B$ interactions for Hole Center *B*. Results are presented for each of the three high-symmetry planes.

one of these sets of nine atoms. There are two additional atoms (denoted by primes) included in Table II that are part of other sets of nine atoms. An important feature of the $LiB_3O_5$ lattice is the existence of both $BO_3$ and $BO_4$ units. These units combine to form $B_3O_7$ anionic groups that are linked to each other in an endless network within the crystal. The seven oxygen atoms and three boron atoms in Table II form one $B_3O_7$ group. In Fig. 9(a), these ten atoms and the adjacent lithium atom are shown in a projection onto the plane defined by the three boron atoms. This plane containing the three boron atoms is not simply related to the *a*, *b*, and *c* axes of the crystal. The normal to this plane is described by $\theta = 54.5°$ and $\phi = 25.1°$, where $\theta$ and $\phi$ are defined in Sec. III. In the view provided in Fig. 9(a), the O(5′) atom is located well above the plane and the O(2′) atom is located well below the plane, while the O(1), O(3), O(4), and Li(1) atoms are slightly above the plane and the O(2) and O(5) atoms are slightly below the plane. Within this $B_3O_7$ group, two of the boron atoms are threefold bonded and one

TABLE II. Fractional coordinates of atoms in $LiB_3O_5$ (given in units of the *a*, *b*, and *c* lattice parameters). The first nine atoms in this table represent one-quarter of a unit cell. Positions of the remaining 27 atoms are obtained from these nine positions by application of the three symmetry elements of the crystal.[a] The last two atoms in this table, each denoted by a prime, are part of other symmetry-generated sets of nine. These three boron and seven oxygen atoms listed below form a $B_3O_7$ group. (This table was constructed using information in Ref. 21.)

| Atom | *x*/*a* | *y*/*b* | *z*/*c* |
|---|---|---|---|
| Li(1) | 0.5873 | 0.4333 | 0.9548 |
| B(1) | 0.9903 | 0.3356 | 0.3098 |
| B(2) | 0.8056 | 0.5567 | 0.5063 |
| B(3) | 0.8430 | 0.2514 | 0.6895 |
| O(1) | 0.9136 | 0.4957 | 0.3022 |
| O(2) | 1.1163 | 0.2951 | 0.1535 |
| O(3) | 0.9419 | 0.2018 | 0.4848 |
| O(4) | 0.7610 | 0.4098 | 0.6902 |
| O(5) | 0.8390 | 0.1250 | 0.8840 |
| O(2′) | 0.8837 | 0.7049 | 0.6535 |
| O(5′) | 0.6610 | 0.6250 | 0.3840 |

[a]The following transformations allow the additional sets of nine atoms to be generated from an initial set (which is arbitrarily labeled Set 1).

Set 1: $(x, y, z)$

Set 2: $(1/2-x, 1/2+y, 1/2+z)$ Reflection through the *a* plane and translation of 1/2 along *b* and *c*.

Set 3: $(1/2+x, 1/2-y, z)$ Reflection through the *b* plane and translation of 1/2 along *a*.

Set 4: $(-x, -y, 1/2+z)$ Sequential application of the two previous transformations and translation of 1/2 along *c*.

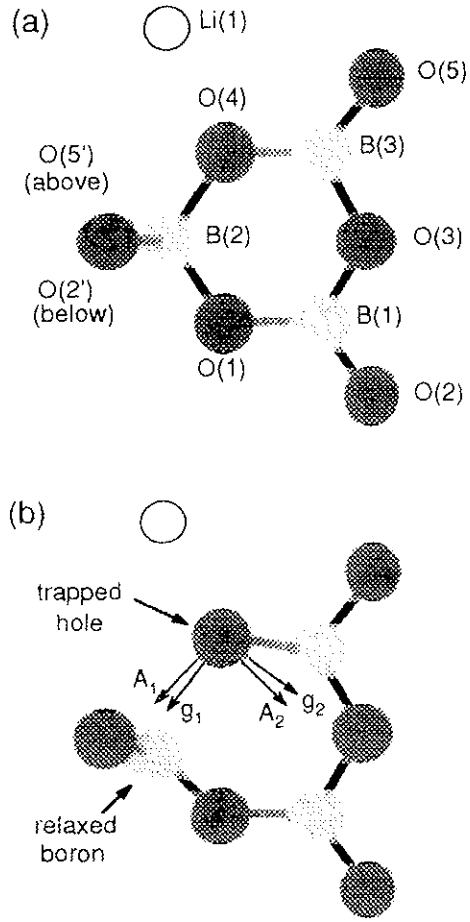


FIG. 9. (a) Schematic representation of the basic $B_3O_7$ anionic group in the $LiB_3O_5$ lattice, projected onto the plane formed by the three boron atoms. Five of the seven oxygen atoms lie close to this plane. A neighboring lithium ion is also close to this plane, and is included. (b) Proposed model of the self-trapped hole center in $LiB_3O_5$. Atom labels are the same as in part (a). The hole is primarily localized on O(4). Both O(4) and B(2) relax from their initial positions, thus allowing the hole to be self-trapped.

boron atom is fourfold bonded.

Several experimental observations must be taken into account when constructing models for the two trapped hole centers in $LiB_3O_5$. The $g$ matrices described in Table I have small, but significant, positive shifts of the order expected for a hole localized primarily on an oxygen ion. In a simple ionic picture (which ignores the high degree of covalency within the borate units in $LiB_3O_5$), the $O^-$ ion that contains the hole would have a $2p^5$ configuration ($2p_x^2$, $2p_y^2$, $2p_z$) with $L=1$, $S=1/2$. The threefold orbital degeneracy of this $^2P$ state of the $O^-$ ion is then removed by the crystalline electric field. In ascending order, the three energy levels would be $E_1$, $E_2$, and $E_3$. Shifts of the principal values from the free-spin value ($g_e=2.0023$) are caused by spin-orbit interactions that admix excited states to the ground state. This very simple analysis (based on the ionic picture) predicts the following $g$ values:

$$g_1 = g_e, \tag{2}$$

$$g_2 = g_e - \frac{2\lambda}{E_3 - E_1}, \tag{3}$$

$$g_3 = g_e - \frac{2\lambda}{E_2 - E_1}. \tag{4}$$

The spin-orbit coupling constant $\lambda$ for the $O^-$ ion is approximately $-135$ cm$^{-1}$. One experimental $g$ value (see Table I) for each of the hole centers is very close to $g_e$, as predicted by Eq. (2). Also, Eqs. (3) and (4) predict small, and different, positive $g$ shifts for the other two $g$ values, in general agreement with experiment. The energy differences appearing in the denominators in Eqs. (3) and (4) are expected to correspond, in an approximate sense, to optical absorption bands associated with the hole centers in the visible and near infrared.

Additional experimental evidence that has a significant influence on the choice of models for the two hole centers comes from the observed hyperfine interactions. Each hole center has a strong interaction with only one boron nucleus. Since every oxygen atom in the $LiB_3O_5$ lattice has two boron neighbors, the initial expectation would have been for a trapped hole to exhibit significant interactions with both of its boron neighbors. A dominant interaction with only one boron can be explained if one of the neighboring boron atoms is missing (i.e., a boron vacancy exists) or if one of the boron atoms undergoes a large relaxation away from the oxygen containing the hole. Our cluster calculations, described later in this section, directly support models based on the large lattice relaxation of one boron neighbor. The boron vacancy model is considered to be a less likely possibility because of the observed low thermal stability of the two trapped hole centers (Hole Center $A$ decays near 130 K and Hole Center $B$ decays between 150 and 200 K).

It is often possible in EPR and ENDOR studies of point defects[23,30,31] to find correlations between the crystalline bond directions and the experimentally determined principal-axis directions of the $g$ and hyperfine matrices, and thus obtain supporting evidence for proposed models. There are, of course, no absolute reasons why a particular principal-axis direction should be close to a bond direction in a low-symmetry crystal that has significant covalency, such as $LiB_3O_5$. Also, a complicating factor in our case is the existence of four crystallographically equivalent sites in the $LiB_3O_5$ lattice for each of the trapped hole centers, and we cannot say with certainty which one of these four sites corresponds to the specific set of parameters in Table I. However, despite these concerns, we did find a strong correlation with the crystal structure for several of the experimental principal-axis directions. We focus on the $B_3O_7$ group illustrated in Fig. 9(a) and arbitrarily label the hole center found in this group as site 1 (and we assign the parameters listed in Table I to the defect site located in this group). The principal axis associated with the unique principal hyperfine value for Hole Center $A$ (i.e., the $-19.84$ MHz value) is almost exactly normal to the plane formed by the three boron atoms in this $B_3O_7$ group. Specifically, it makes an angle of 0.7° with this normal. Le Henaff *et al.*[23] have shown that there is a $\pi$-electron transfer from the oxygen atoms to the $p_z$ orbitals of the threefold-bonded boron atoms in $LiB_3O_5$. This $\pi$ molecular orbital will transfer spin density to the boron when a hole is trapped on the adjacent oxygen, and the resulting anisotropic hyperfine (i.e., dipole-dipole) interaction will be controlled, in large part, by the partially occupied $p_z$ orbital of the boron in the planar $BO_3$ unit.[32] These observations provide experimental verification that the large $^{11}$B hyperfine observed in both Hole Center $A$ and Hole Center $B$ is with a threefold-bonded boron atom, and suggest that the boron atom undergoing the large relaxation (see the previous paragraph) is fourfold bonded. Turning to the principal-axis directions for the $g$ matrix of Hole Center $A$, we find additional correlations with the $B_3O_7$ group in Fig. 9(a). The direction of the largest $g$ value (i.e., the 2.0456 value) makes an angle of 4.3° with the normal to the plane formed by the three boron atoms in this $B_3O_7$ group, and the direction of the smallest $g$ value (i.e., the 2.0021 value) makes an angle of 6.3° with the line joining the O(4) and B(2) atoms.

The GAUSSIAN 98 *ab-initio* molecular orbital computer program[33] has helped to clarify the electronic and atomic structure of the trapped hole centers in $LiB_3O_5$. The cluster approach to the calculation of the electronic structure of point defects in insulators has recently been described in detail by Pacchioni *et al.*[34] A $(B_3O_7H_4)^0$ cluster, consisting of one $BO_4$ and two $BO_3$ units along with four hydrogens to terminate the outer oxygens, was selected for our calculations. This cluster contains 75 electrons and represents the basic anionic group illustrated in Fig. 9(a). The four hydrogens were placed 0.98 Å from oxygens O(2), O(5), O(2′), and O(5′) with their directions aligned along the oxygen-boron bonds they replace. A 6-31G basis set was used in our unrestricted Hartree-Fock electronic structure calculations.[35] The initial calculation was done with the three boron and seven oxygen atoms fixed at positions that duplicated the regular lattice. Then a series of geometry-optimization calculations were performed in which only one atom was allowed to move per calculation. These GAUSSIAN 98 results are summarized in Table III.

TABLE III. Summary of GAUSSIAN 98 results for the $(B_3O_7H_4)^0$ cluster. For comparison purposes, the experimental results in Table I give a Fermi contact value of −30.95 MHz for the primary boron hyperfine interaction for Hole Center *A*.

| Geometry-optimized? | Ion moved | Total energy (Hartree) | Fermi contact (MHz) B(1) | B(2) | B(3) |
|---|---|---|---|---|---|
| No | None | −600.4692 | −6.36 | −40.03 | −40.31 |
| Yes | B(3) | −600.4887 | −3.34 | −28.26 | −26.22 |
| Yes | B(2) | −600.5288 | −1.97 | −13.38 | −40.01 |
| Yes | O(4) | −600.5459 | −1.97 | −3.62 | −52.50 |

All of our GAUSSIAN 98 calculations show the hole to be primarily localized on a single oxygen, specifically O(4) in Fig. 9(a). The distinguishing features of each calculation are the total energy and the relative values of the Fermi contact parameter for the three boron atoms. In Table III, the first entry is the calculation done with all of the boron and oxygen atoms fixed at their regular positions. In this case, the Fermi contact values for the two boron atoms neighboring the hole are large and nearly equal. This clearly does not agree with experiment. In the second entry in Table III, the threefold-bonded boron B(3) was allowed to move while the other atoms remained at their regular positions. The minimum energy is reached when B(3) has moved 0.16 Å from its initial position, in the direction between O(3) and O(5) and away from O(4). This cluster, with B(3) relaxed, still gives nearly equal, although smaller, Fermi contact values for the two boron atoms adjacent to the hole, and thus does not agree with experiment. In the third entry in Table III, the fourfold-bonded boron B(2) was allowed to move while the other atoms were fixed in their regular lattice positions. The minimum energy is reached when B(2) has moved 0.38 Å from its starting position, in the direction between O(1), O(2′), and O(5′) and again away from O(4). This relaxation places B(2) nearly in the plane of O(1), O(2′), and O(5′), and effectively converts B(2) from being fourfold bonded to being threefold bonded. After B(2) relaxes, the Fermi contact parameters for the two boron atoms are no longer nearly equal. In our final calculation, described by the fourth entry in Table III, O(4) was allowed to move while B(2) was fixed at its final optimized position (reached in the previous step) and all the other atoms were fixed at their original lattice positions. A minimum energy occurs when O(4) has moved 0.31 Å from its starting position in the direction away from B(2). The distance between O(4) and B(2) has increased to 2.05 Å in this final relaxed configuration, compared to an initial unrelaxed separation of 1.49 Å, while the distance between O(4) and B(3) has only increased to 1.39 Å in the final configuration, compared to an initial unrelaxed separation of 1.36 Å. Also, the Fermi contact value for B(3) is now more than an order of magnitude larger than the Fermi contact value for B(2). These relative values are now in good agreement with experiment. The final relaxed configuration predicted by our GAUSSIAN 98 calculations is shown in Fig. 9(b).

Our GAUSSIAN 98 calculations show that a large relaxation of the nearest-neighbor fourfold-bonded boron will accompany the localization of a hole on one oxygen in the $LiB_3O_5$ lattice. Both Hole Center *A* and Hole Center *B* have this lattice distortion, which in each case is demonstrated by the observation of only one dominant boron hyperfine interaction. To distinguish between Hole Center *A* and Hole Center *B*, we need to focus on the difference in the stabilizing mechanism for each center. The observation (see Fig. 5) that a nearby lithium ion participates in Hole Center *A* supports a self-trapped model for this center. With the magnetic field along the *a* axis of the crystal, we found a $^7$Li hyperfine splitting of 5.83 MHz. This large value indicates that the nearest-neighbor lithium ion shown in Fig. 9(a) is present in Hole Center *A*, and that there is not an adjacent lithium vacancy to provide a stabilizing force for Hole Center *A*. Hence, the large relaxation predicted by the GAUSSIAN 98 calculations is the only stabilizing (i.e., trapping) influence for this center. Hole Center *B*, on the other hand, should have a stabilizing entity (since two separate self-trapped hole centers are not expected), and a lithium vacancy is the prime candidate for this neighboring defect. We note that the data in Fig. 2 shows the presence of the trapped electron center in our $LiB_3O_5$ crystals, and this allows us to conclude that our crystals contain oxygen vacancies. If oxygen vacancies are present, then lithium vacancies must also be present because these two vacancies are expected to provide charge compensation for each other in the as-grown crystals (there are no known impurities present at significant concentrations to serve in this role). Since lithium vacancies are almost certainly in our crystals, we consider it reasonable to assign a model to Hole Center *B* that includes a lithium vacancy as the stabilizing entity.

## V. SUMMARY

Two similar trapped hole centers, labeled Hole Center *A* and Hole Center *B*, have been investigated in single crystals of $LiB_3O_5$. Hole Center *A* is observed after the crystals are irradiated at 77 K with x rays, and Hole Center *B* is observed after the irradiated crystals are annealed to 130 K. A complete set of spin-Hamiltonian parameters is determined for each of the centers, including the *g* matrix and the $^{11}$B hyperfine and nuclear quadrupole matrices. In both of these hole centers, a hyperfine interaction with one $^{11}$B nucleus dominates the EPR spectra. We suggest that Hole Center *A* is a self-trapped hole center (i.e., the hole is stabilized on one oxygen as a result of a significant relaxation in the surrounding lattice, with no other point defects nearby). Four out of the five inequivalent oxygen atoms in the $LiB_3O_5$ lattice have a threefold bonded boron neighbor and a fourfold bonded boron neighbor. When a hole is localized on one of these oxygen atoms, the boron atom that was initially fourfold bonded relaxes a large distance away from the hole and forms an "effective" planar threefold bonded unit with its remaining three oxygen neighbors and contributes to the lowering of the total energy for the defect. The hole is left to interact significantly only with its initial threefold bonded boron neighbor. This model is extended in the case of Hole Center *B* to include a neighboring lithium vacancy. Hole

Center *A* and Hole Center *B* have very similar spin-Hamiltonian parameters, thus their structures must be similar. We suggest that the large lattice relaxation proposed for Hole Center *A* also occurs for Hole Center *B*, and that the neighboring lithium vacancy simply provides additional thermal stability for Hole Center *B*.

A major goal of our present study was to understand the point defects that participate in the transient optical absorptions produced in $LiB_3O_5$ when these crystals are used in frequency conversion applications involving ultraviolet beams from high-power pulsed lasers. Our self-trapping model for the dominant low-temperature hole center suggests that this defect will be formed in every $LiB_3O_5$ crystal and, because of its intrinsic nature, cannot be eliminated simply by improvements in crystal growth. However, the "steady-state" concentration of self-trapped holes formed during operation of ultraviolet devices should be considerably decreased if efforts are made to reduce the number of oxygen vacancies that serve as the corresponding primary electron trap in this lattice. Without a long-lived electron trap, the self-trapped holes will have very short lifetimes, and significant concentrations cannot build up on millisecond time scales. Thus, we suggest that modifications in the crystal growth process designed to minimize the number of oxygen vacancies may help alleviate problems arising from transient ultraviolet absorption bands in nonlinear optical devices utilizing $LiB_3O_5$.

## ACKNOWLEDGMENTS

This work was supported at West Virginia University by the Air Force Office of Scientific Research (Grant No. F49620-00-1-0301). The authors wish to thank K. T. Stevens for performing x-ray orientations of the $LiB_3O_5$ crystals.

*Electronic address: Larry.Halliburton@mail.wvu.edu

[1] W. Koechner, *Solid-State Laser Engineering*, 5th ed. (Springer, Berlin, 1999), Chap. 10, pp. 582–666.
[2] D.N. Nikogosyan, Appl. Phys. A: Solids Surf. **58**, 181 (1994).
[3] I.N. Ogorodnikov, A.V. Porotnikov, S.V. Kudyakov, and A.V. Kruzhalov, Phys. Solid State **39**, 1366 (1997).
[4] M.P. Scripsick, X.H. Fang, G.J. Edwards, L.E. Halliburton, and J.K. Tyminski, J. Appl. Phys. **73**, 1114 (1993).
[5] A.Yu. Kuznetsov, A.B. Sobolev, I.N. Ogorodnikov, and A.V. Kruzhalov, Phys. Solid State **36**, 1876 (1994).
[6] A.V. Porotnikov, I.N. Ogorodnikov, S.V. Kudyakov, A.V. Kruzhalov, and S.L. Votyakov, Phys. Solid State **39**, 1224 (1997).
[7] I.N. Ogorodnikov, A.V. Porotnikov, A.V. Kruzhalov, and V.Yu. Yakovlev, Phys. Solid State **40**, 1817 (1998).
[8] I.N. Ogorodnikov, A.V. Kruzhalov, E.A. Radzhabov, and L.I. Isaenko, Phys. Solid State **41**, 197 (1999).
[9] I.N. Ogorodnikov, V.A. Pustovarov, A.V. Kruzhalov, L.I. Isaenko, M. Kirm, and G. Zimmerer, Phys. Solid State **42**, 464 (2000).
[10] I.N. Ogorodnikov and A.V. Kruzhalov, Russ. Phys. J. **43**, 225 (2000).
[11] I.N. Ogorodnikov, V.A. Pustovarov, M. Kirm, A.V. Kruzhalov, and L.I. Isaenko, Phys. Solid State **43**, 1454 (2001).
[12] I.N. Ogorodnikov, L.I. Isaenko, A.V. Kruzhalov, and A.V. Porotnikov, Radiat. Meas. **33**, 577 (2001).
[13] Y.-N. Xu and W.Y. Ching, Phys. Rev. B **41**, 5471 (1990).
[14] R.H. French, J.W. Ling, F.S. Ohuchi, and C.T. Chen, Phys. Rev. B **44**, 8496 (1991).
[15] W.Y. Hsu and R.V. Kasowski, J. Appl. Phys. **73**, 4101 (1993).
[16] Y.-N. Xu, W.Y. Ching, and R.H. French, Phys. Rev. B **48**, 17 695 (1993).
[17] A.B. Sobolev, A.Yu. Kuznetsov, I.N. Ogorodnikov, and A.V. Kruzhalov, Phys. Solid State **36**, 829 (1994).
[18] A.Yu. Kuznetsov, A.B. Sobolev, I.N. Ogorodnikov, and A.V. Kruzhalov, Radiat. Eff. Defects Solids **134**, 69 (1995).
[19] J. Li, C. Duan, Z. Gu, and D. Wang, Phys. Rev. B **57**, 6925 (1998).
[20] C. Duan, J. Li, Z. Gu, and D. Wang, Phys. Rev. B **60**, 9435 (1999).
[21] S.F. Radaev, B.A. Maximov, V.I. Simonov, B.V. Andreev, and V.A. D'Yakov, Acta Crystallogr., Sect. B: Struct. Sci. **B48**, 154 (1992).
[22] C. Le Henaff, N.K. Hansen, J. Protas, and G. Marnier, Acta Crystallogr., Sect. B: Struct. Sci. **B53**, 870 (1997).
[23] J.-M. Spaeth, J.R. Niklas, and R.H. Bartram, *Structural Analysis of Point Defects in Solids* (Springer-Verlag, Berlin, 1992).
[24] O.F. Schirmer, J. Phys. Chem. Solids **32**, 449 (1971).
[25] O.F. Schirmer, J. Phys. C **6**, 300 (1973).
[26] Y. Chen and M.M. Abraham, J. Phys. Chem. Solids **51**, 747 (1990).
[27] C.J. Walsby, N.S. Lee, W.C. Tennant, and R.F.C. Claridge, J. Phys.: Condens. Matter **12**, 1441 (2000).
[28] R.H.D. Nuttall and J.A. Weil, Can. J. Phys. **59**, 1696 (1981).
[29] F.J. Adrian, A.N. Jette, and J.M. Spaeth, Phys. Rev. B **31**, 3923 (1985).
[30] J.A. Weil, J.R. Bolton, and J.E. Wertz, *Electron Paramagnetic Resonance: Elementary Theory and Practical Applications* (Wiley, New York, 1994).
[31] M. Symons, *Chemical and Biochemical Aspects of Electron-Spin Resonance Spectroscopy* (Wiley, New York, 1978).
[32] D.L. Griscom, P.C. Taylor, D.A. Ware, and P.J. Bray, J. Chem. Phys. **48**, 5158 (1968).
[33] M.J. Frisch, G.W. Trucks, H.B. Schlegel, G.E. Scuseria, M.A. Robb, J.R. Cheeseman, V.G. Zakrzewski, J.A. Montgomery, R.E. Stratmann, J.C. Burant, S. Dapprich, J.M. Millam, A.D. Daniels, K.N. Kudin, M.C. Strain, O. Farkas, J. Tomasi, V. Barone, M. Cossi, R. Cammi, B. Mennucci, C. Pomelli, C. Adamo, S. Clifford, J. Ochterski, G.A. Petersson, P.Y. Ayala, Q. Cui, K. Morokuma, D.K. Malick, A.D. Rabuck, K. Raghavachari, J.B. Foresman, J. Cioslowski, J.V. Ortiz, B.B. Stefanov, G. Liu, A. Liashenko, P. Piskorz, I. Komaromi, R. Gomperts, R.L. Martin, D.J. Fox, T. Keith, M.A. Al-Laham, C.Y. Peng, A. Nanayakkara, C. Gonzalez, M. Challacombe, P.M.W. Gill, B.G. Johnson, W. Chen, M.W. Wong, J.L. Andres, M. Head-Gordon, E.S. Replogle, and J.A. Pople, GAUSSIAN 98 (Revision A.1) (Gaussian, Inc., Pittsburgh, PA, 1998).
[34] G. Pacchioni, F. Frigoli, D. Ricci, and J.A. Weil, Phys. Rev. B **63**, 054102 (2000).
[35] J. Simons and J. Nichols, *Quantum Mechanics in Chemistry* (Oxford University Press, New York, 1997), Chap. 18, pp. 411–417.